PERFORMANCE OPTIMIZATION OF PMSM DRIVES USING PI-LESS MODEL PREDICTIVE CURRENT CONTROL

BACH THANH QUY[1,*], VAN THI KIEU NHI[1], NGUYEN DAI VI[1]
[1] *Faculty of Electrical Engineering Technology, Industrial University of Ho Chi Minh City*
* *Corresponding author: bachthanhquy@iuh.edu.vn*

Abstract. This paper proposes a novel predictive current control strategy for permanent magnet synchronous motor (PMSM) drives that eliminates the proportional-integral (PI) regulator to reduce the computational burden commonly associated with conventional model predictive current control (MPCC). The controller is derived from the PMSM mathematical model and discretized using the forward Euler method, enabling direct selection of the optimal inverter voltage vector without a PI stage. By removing the PI regulator, the proposed PI-less MPCC reduces computation time while maintaining satisfactory current regulation and torque smoothness. The proposed approach is evaluated on a 1.5 kW PMSM drive model implemented in MATLAB/Simulink. Comparative results against the conventional MPCC show a substantial reduction in computational effort: under the same operating conditions, the total execution time is reduced from 62 s to 11 s. In addition, the proposed method improves speed tracking and significantly reduces overshoot during speed reference changes and load disturbances. These results indicate that the PI-less MPCC achieves a favorable trade-off between computational efficiency and control performance, which makes it a promising candidate for practical PMSM drive applications.

Keywords. permanent magnet synchronous motor, model predictive current control, computational burden, optimal voltage vector.

1 INTRODUCTION

Over the past decades, permanent magnet synchronous motors (PMSMs) have become a preferred solution for modern drive systems because of their high efficiency, high torque density, and high power factor [1, 2]. These characteristics make PMSMs particularly attractive for industrial applications such as railways, electric vehicles, and servo drives [3, 4].

Despite these advantages, high-performance PMSM drives remain challenging because of nonlinear dynamics and tight requirements on torque and stator current regulation [5, 6]. Several control algorithms have been developed for PMSM drives, including Field Oriented Control (FOC) [7, 8], Direct Torque Control (DTC) [9, 10], Sliding Mode Observer Control (SMOC) [11, 12], and Model Predictive Control (MPC) [13, 14]. Among these approaches, MPC is widely recognized as a flexible framework because multiple control objectives can be incorporated into a single optimization problem. In MPC, the future behavior of the drive is predicted using a discrete-time model, and the optimal voltage vector of the voltage-source inverter is selected by minimizing a predefined cost function at each sampling interval. This predictive optimization framework can reduce current ripples, enhance torque regulation, and improve overall drive performance. Depending on the selected control variables, MPC-based PMSM control can be classified into Model Predictive Flux Control (MPFC) [15, 16], Model Predictive Speed Control (MPSC) [17, 18], Model Predictive Torque Control (MPTC) [19, 20], and Model Predictive Current Control (MPCC) [21, 22]. The MPCC is the most widely adopted variant because it provides direct current regulation and is well suited for incorporating inverter switching constraints. However, MPCC can still exhibit residual torque ripple, degraded performance under rapid load variations, and sensitivity to model inaccuracies and parameter mismatches, which may affect robustness and stability in practical implementations [23]. In addition, practical MPCC implementations are frequently integrated with PI-based regulation stages, which increases tuning complexity and computational burden under strict real-time constraints.

Motivated by this issue, this paper proposes a PI-less MPCC strategy that preserves the predictive current control principle of conventional MPCC while eliminating the PI regulation stage. By removing the PI block, the proposed approach reduces computational cost and tuning effort while improving transient speed behavior, particularly by suppressing overshoot during speed and load changes.

© 2026 Industrial University of Ho Chi Minh City

The main contributions of this paper are summarized as follows:

a) A PI-less MPCC scheme is developed for PMSM drives, which retains the predictive current control mechanism of conventional MPCC while eliminating the PI regulation stage, thereby simplifying tuning and reducing implementation complexity.

b) The proposed PI-less structure substantially lowers computational effort. In MATLAB/Simulink simulations, the total execution time is reduced from 62 s (conventional MPCC) to 11 s (PI-less MPCC), corresponding to an approximate 82.3% reduction.

c) During motor start-up and speed ramp-up, the proposed PI-less MPCC reduces the overshoot in stator current, speed, and electromagnetic torque by approximately 50% compared with the conventional MPCC, while maintaining accurate current tracking and stable operation.

The remainder of this paper is organized as follows. Section 2 presents the theoretical background of the research, including the PMSM model, the two-level voltage source inverter, and the conventional MPCC formulation. Section 3 presents the proposed PI-less MPCC, including the prediction model, cost function, and switching-state selection procedure. Section 4 reports MATLAB/Simulink simulation results and comparisons under speed and load transients. Section 5 concludes the paper.

2 THEORETICAL BACKGROUND AND CONVENTIONAL MODEL PREDICTIVE CURRENT CONTROL

2.1. PMSM mathematical model

The PMSM model is constructed in the synchronous rotating direct-quadrature (dq) reference frame derived from space vector theory as stated in [24], assuming hysteresis losses are ignored. By applying the Clarke-Park transformation, the three-phase (abc) stator voltage equations are mapped to an equivalent dq -axis system. The dq-reference frame follows the rotor and rotates at the electrical synchronous speed ω_e, separating the flux and torque generating components. Stator voltages are neatly represented in terms of dynamics as follows:

$$\begin{cases} u_d = R_s i_d + L_d \frac{di_d}{dt} - \omega_e L_q i_q \\ u_q = R_s i_q + L_q \frac{di_q}{dt} + \omega_e L_d i_d + \omega_e \varphi_f \end{cases} \quad (1)$$

where u_d and u_q are the dq-axis stator voltages; i_d and i_q represent the dq -axis stator currents; L_d and L_q correspond to the dq-axis inductances; the stator resistance is R_s and the synchronous electrical angular speed is ω_e; φ_f is the permanent magnet flux linkage. By rearranging (1), the PMSM model can be written in the stator current state form as:

$$\begin{cases} \frac{di_d}{dt} = -\frac{R_s}{L_d} i_d + \omega_e \frac{L_q}{L_d} i_q + \frac{1}{L_d} u_d \\ \frac{di_q}{dt} = -\frac{R_s}{L_q} i_q - \omega_e \frac{L_d}{L_q} i_d + \frac{1}{L_q} u_q - \omega_e \frac{\varphi_f}{L_q} \end{cases} \quad (2)$$

The stator flux linkages in the rotating frame are given by:

$$\begin{cases} \varphi_d = L_d i_d + \varphi_f \\ \varphi_q = L_q i_q \end{cases} \quad (3)$$

where φ_d and φ_q denote the stator flux components along the dq-axis. Accordingly, the electromagnetic torque can be expressed as:

$$T_e = \frac{3}{2} p \, (\varphi_d i_q - \varphi_q i_d) \quad (4)$$

where p is the number of pole pairs.

The mechanical dynamics of the motor shaft are described by the torque balance equation:

$$T_e - T_L = J \frac{d\omega_m}{dt} + B_m \omega_m \quad (5)$$

here ω_m is the rotor mechanical speed; T_L is the load torque; J and B_m are the rotor inertia and viscous friction coefficient, respectively. The electrical and mechanical speeds satisfy $\omega_e = p\omega_m$

2.2. Two-level Voltage Source Inverter (VSI)

In the model predictive control algorithm, the two-level voltage source inverter (VSI) is used to provide three-phase power for the PMSM. The VSI consists of a DC-link voltage source and six power semiconductor devices arranged in three half-bridges to generate controlled three-phase voltages at the machine terminals. The three-leg switch pairs are denoted (S_a, $\overline{S}_a$), (S_b, $\overline{S}_b$), and (S_c, $\overline{S}_c$), where each device is equipped with an anti-parallel diode to ensure current commutation under inductive load conditions. The circuit of the three-phase VSI and eight voltage vectors ($V_i(S_a S_b S_c); i = 0, \dots, 8$) generated by the inverter switching states are illustrated in Figs. 1 and 2.

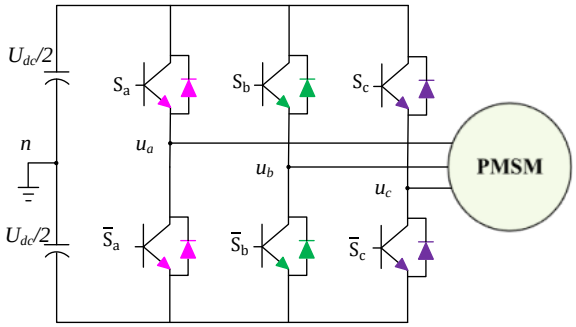


Figure 1: The circuit of the three-phase VSI

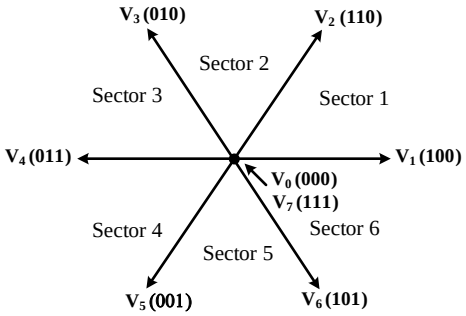


Figure 2: Voltage vectors of the VSI

The two-level VSI supplies the PMSM with continuous voltages in the rotating dq-reference frame via the following equations:

$$\begin{bmatrix} u_d \\ u_q \end{bmatrix} = \frac{2}{3} V_{dc} \begin{bmatrix} cos\theta_e & \cos(\theta_e - \frac{2\pi}{3}) & \cos(\theta_e + \frac{2\pi}{3}) \\ -sin\theta_e & -sin(\theta_e - \frac{2\pi}{3}) & -sin(\theta_e + \frac{2\pi}{3}) \end{bmatrix} \begin{bmatrix} S_a \\ S_b \\ S_c \end{bmatrix} \quad (6)$$

in which $\boldsymbol{\theta_e}$ is the electrical angular.

2.3. The Conventional Model Predictive Current Control Strategy

The objective of MPCC for PMSM drives is to guarantee precise tracking of the reference d-q axis currents. MPCC improves dynamic response and reduces current distortion and torque ripple by predicting the future currents associated with each candidate voltage vector and minimizing the corresponding cost function. In addition, the method can improve system stability and reduce the effect of disturbances by lowering current THD and torque ripple. The workflow of the conventional method can be described as follows. First, the three-phase current of the PMSM is transformed to the reference dq-axis currents at the current step using the Clarke-Park transformation. Then, the current at the next sampling step is predicted for each candidate voltage vector of the VSI based on the current error. A current cost function is defined, representing the error between the predicted current and the reference current across all voltage vectors. The voltage vector that minimizes the cost function is selected as the optimal switching state for the next control interval. The flowchart and MATLAB/Simulink diagram of the method are presented in Figs. 3 and 4.

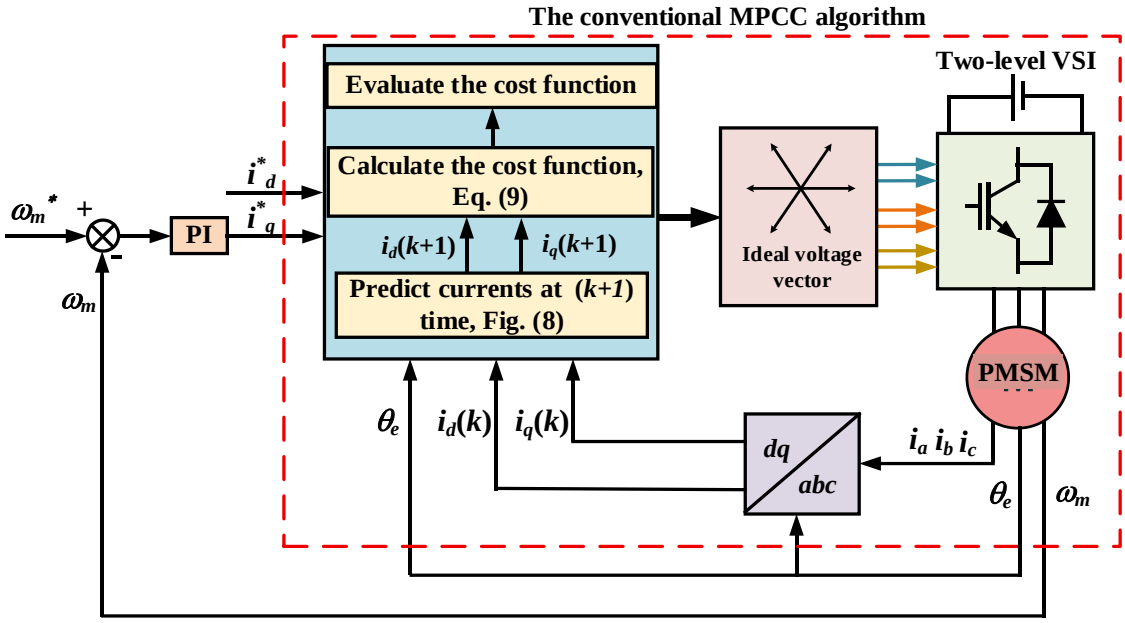


Figure 3: The block diagram of the conventional MPCC

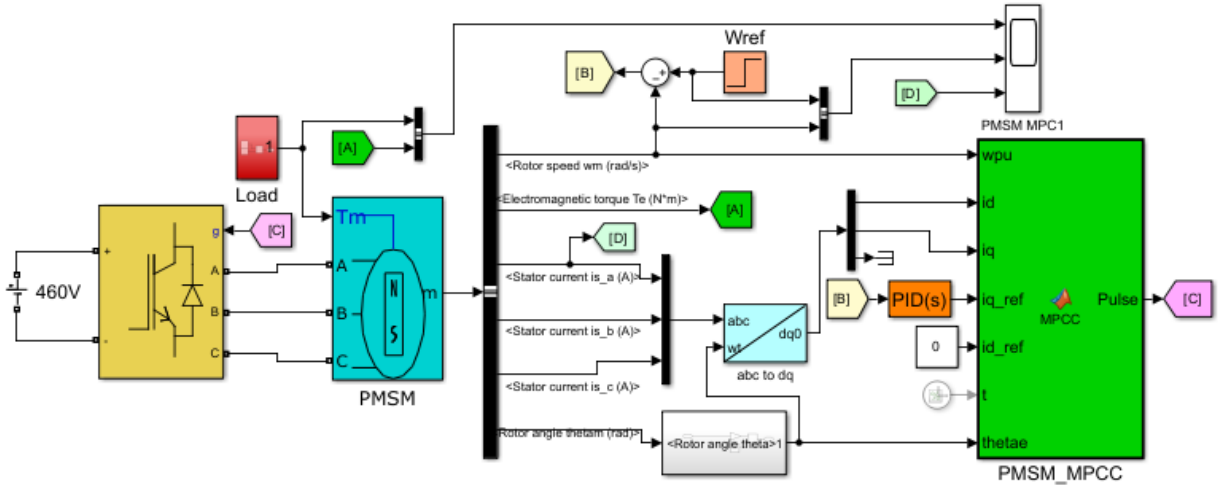


Figure 4: The MATLAB/Simulink diagram of the conventional MPCC

This algorithm is determined based on the following equation:

$$\begin{cases} \frac{di_d(t)}{dt} = \frac{i_d(k+1)-i_d(k)}{T_s} \\ \frac{di_q(t)}{dt} = \frac{i_q(k+1)-i_q(k)}{T_s} \end{cases} \quad (7)$$

in which T_s is the sample period; k and $k+1$ are the k^{th} current control instant and the $(k+1)^{th}$ next instant of the VSI controller; $i_d(k+1)$ and $i_q(k+1)$ are the predicted currents along the dq-axis at the $(k+1)^{th}$ instant; $i_d(k)$ and $i_q(k)$ are the currents along the dq-axis at the k^{th} current control time instant. From (2) and (7), the predictive currents at the $(k+1)^{th}$ instant can be expressed as:

$$\begin{cases} i_d(k+1) = \left(1-\frac{R_s T_s}{L_d}\right) i_d(k) + \omega_e(k)\frac{L_q T_s}{L_d} i_q(k) + \frac{T_s}{L_d} u_d(k) \\ i_q(k+1) = -\omega_e(k)\frac{L_d T_s}{L_q} i_d(k) + \left(1-\frac{R_s T_s}{L_q}\right) i_q(k) + \frac{T_s}{L_q} u_q(k) - \omega_e(k)\frac{\varphi_f T_s}{L_q} \end{cases} \quad (8)$$

where $\omega_e(k)$ is the electrical angular speed at the k^{th} current control time.
The cost function of the conventional MPCC for a PMSM is built based on current tracking objectives.

Specifically, the tracking term is constructed from the mismatch between the predicted dq-axis currents and their corresponding reference values. By evaluating this error at each sampling instant, the controller selects the switching state that drives the predicted currents as close as possible to the references, thereby suppressing current ripple and mitigating fluctuations. In accordance with [25], the cost function F_1can be written as:

$$F_1 = (i_d^* - i_d(k+1))^2 + (i_q^* - i_q(k+1))^2 \quad (9)$$

where i_d^* and i_q^* are the reference dq -axis current elements. All candidate voltage vectors generated by the VSI are evaluated within the optimization routine. The vector creating the minimum value of the cost function is then selected as the optimal switching state and applied to the PMSM during the next period. Conventional MPCC reduces current THD and torque fluctuation, thereby improving PMSM drive performance.

3 THE PI-LESS MODEL PREDICTIVE CURRENT CONTROL

As presented in Section 2.3, the conventional MPCC scheme is implemented with a two-loop structure: an outer-loop PI regulator and an inner-loop MPCC algorithm embedded in a MATLAB Function block. In this architecture, the PI regulator generates the q-axis current reference i_q^* from the speed tracking error, the difference between the measured motor speed and the reference speed. However, the PI action depends directly on the proportional gain k_P and integral gain k_I, whose tuning is often time-consuming and nontrivial during practical commissioning and operation. These characteristics indicate that the conventional approach incurs both additional computational burden and increased tuning complexity of the PI parameters. Such drawbacks may limit its suitability for high-performance drive applications where fast computation and straightforward parameterization are required.

To address these issues, this study proposes a PI-less MPCC strategy for PMSM drives by eliminating the outer-loop PI regulator. Removing the PI stage significantly reduces computational time and simplifies the controller structure. Consequently, the proposed controller can track the reference more effectively, which helps mitigate overshoot during motor start-up and under speed transitions. This subsection presents the design procedure of the proposed method, including the control algorithm formulation, the corresponding block diagram, and the MATLAB/Simulink implementation of the proposed scheme. The detailed description is provided as follows.

Replacing (3) with (4), the electromagnetic torque is rewritten as follows:

$$T_e = \frac{3}{2} p\ (\varphi_f i_q + (L_d - L_q) i_q i_d) \quad (10)$$

To simplify the analysis, assume that $L_d = L_q$ for a surface-mounted PMSM and neglect mutual inductance coupling. With these assumptions, the machine model in (10) is reformulated as:

$$T_e = \frac{3}{2} p\ \varphi_f i_q \quad (11)$$

Alternatively, the dq-axis current components can be expressed in terms of the phase current i_p and the electrical angle θ_e as follows:

$$\begin{cases} i_q = i_p cos\theta_e \\ i_d = -i_p sin\theta_e \end{cases} \quad (12)$$

For improved PMSM performance, electromagnetic torque oscillation should be minimized. From (11) and (12), we can obtain:

$$-\frac{3}{2} p\ \varphi_f i_p sin\theta_e = 0 \quad (13)$$

$$i_d = 0 \quad (14)$$

In contrast, the proposed cost function is constructed directly from the speed-tracking error instead of the current-tracking error, thus eliminating the PI block in the algorithm.

$$F_2 = (\omega_m^* - \omega_m(k+1))^2 \quad (15)$$

where ω_m^* is the reference mechanical speed; $\omega_m(k+1)$ is the predicted speed calculated as (16)

$$\omega_m(k+1) = \frac{3p\varphi_f}{2J} \int_k^{k+1} i_q\, dt - \frac{(L_q - L_d)}{J} \int_k^{k+1} i_q\, i_d dt - \frac{1}{J} \int_k^{k+1} T_L\, dt + \omega_m(k) \quad (16)$$

The predicted speed is discretized using the forward Euler method.

$$\omega_m(k+1) = \frac{3p\varphi_f T_s}{4J}\left(i_q(k+1) - i_q(k)\right) - \frac{T_L T_s}{J} + \omega_m(k) \quad (17)$$

The proposed objective function in (15) quantifies the tracking error between the predicted rotor speed and the reference speed. At each sampling instant, this cost is evaluated for all eight candidate voltage vectors of the VSI. The switching state that yields the minimum cost is then selected and applied to the PMSM during the subsequent control interval. Consequently, the proposed control strategy fully eliminates the need for a PI speed regulator. PI-less MPCC implementations are illustrated in Figs. 5 and 6.

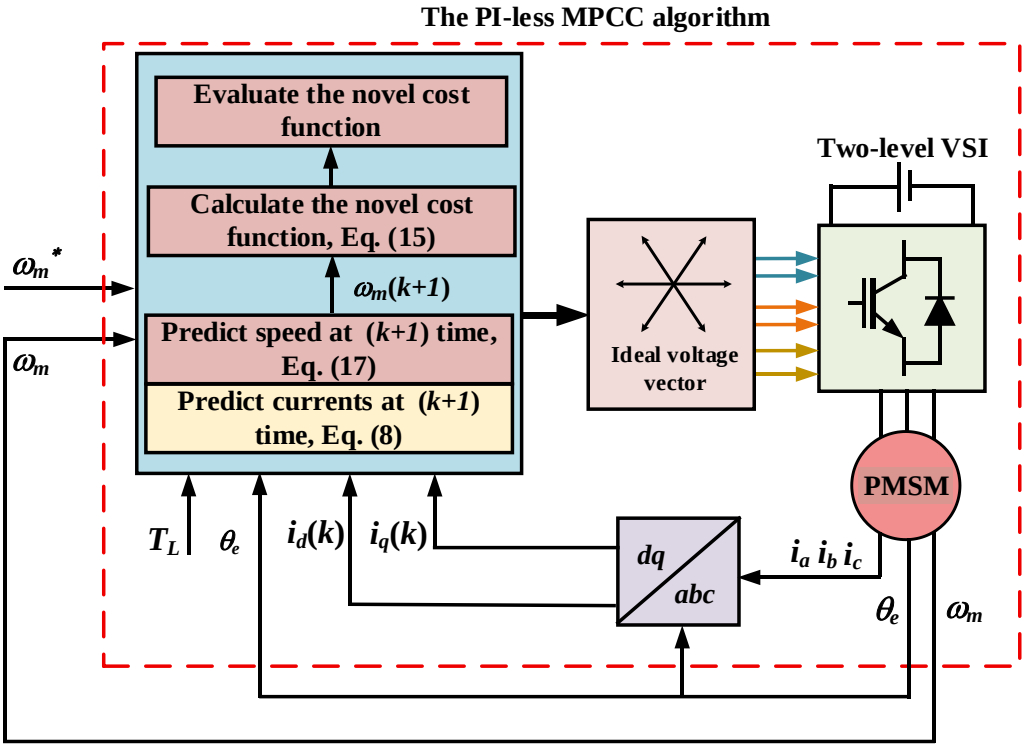


Figure 5: The block diagram of the PI-less MPCC

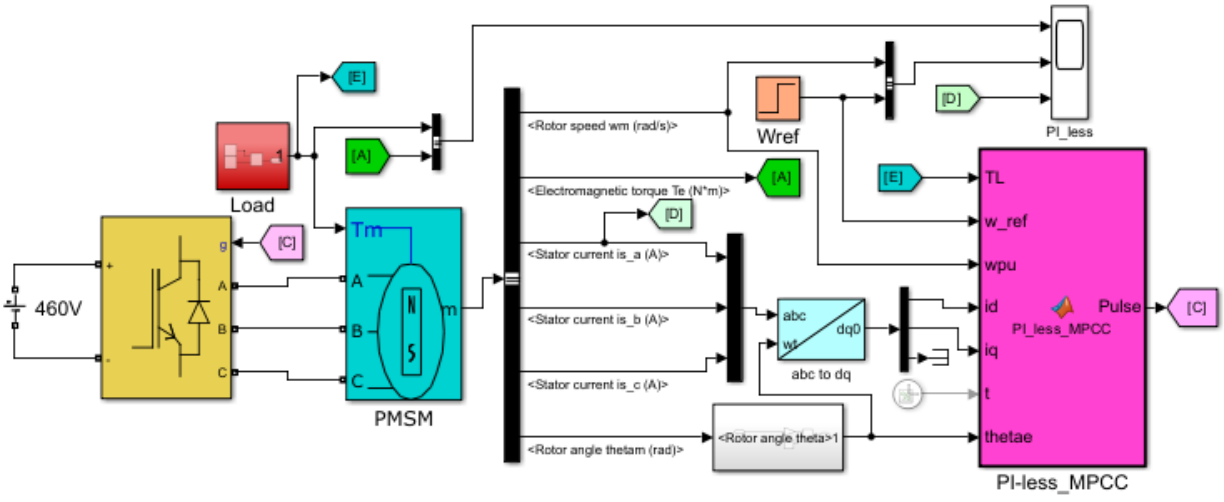


Figure 6: The MATLAB/Simulink diagram of the PI-less MPCC

4 RESULTS AND DISCUSSION

The performance of the PI-less MPCC method is tested and compared with the conventional MPCC using MATLAB/Simulink. For a comprehensive discussion, this paper includes the following verification steps. First, both algorithms are tested using MATLAB/Simulink with a sampling time $T_s = 10^{-5}s$. Also,

simulation results of the current total harmonic distortion, electromagnetic torque response, speed, and dq-axis currents of the PMSM are illustrated for both steady-state and dynamic modes. Lastly, to demonstrate the superiority of the proposed strategy over the classical approach, the results of the two methods are analyzed and compared. The motor and control parameters of the PMSM are shown in Table 1. The verification procedures for the traditional method and the proposed PI-less MPCC method are as follows. The motor starts from rest and accelerates to 70 rad/s. The load torque is then stepped from 10 Nm to 20 Nm at t = 0.15 s, reduced to 5 Nm afterward, and the speed reference is changed to 80 rad/s at t = 0.3 s.

Table 1. The motor and control parameters of the PMSM

Parameters	Value
Rated Power P_r (kW)	1.5
Rated Speed n_r (rpm)	750
Pole pairs	4
Stator resistance R_s (Ω)	0.11
Total inertia j (kg.m^2)	0.0016
DC-link voltage U_{dc} (V)	460
d-axis inductance L_d (H)	0.00097
q-axis inductance L_q (H)	0.00097
Rotor peak PM flux linkage φ_f(Wb)	0.1119
Rated torque T_r (N.m)	20
Switching frequency f_s (kHz)	100

4.1. PMSM's steady-state performance evaluation

In this section, the motor's steady-state operation is evaluated under a load condition requiring a shaft torque of 10 Nm and a speed of 70 rad/s, applied at 0.05 s. The outcomes of the two methods are presented in Figs. 7 and 8, comparing the stator-current total harmonic distortion (THD) and the electromagnetic torque responses, respectively.

Fig. 7 compares the phase current waveform and its harmonic spectrum obtained with the conventional MPCC (Fig. 7(a)) and the PI-less MPCC (Fig. 7(b)). In the time domain, both controllers produce a quasi-sinusoidal current with very similar peak values (+19.2 A and -19.5 A for the MPCC, +19.2 A and -19.3 A for the PI-less MPCC), indicating comparable current tracking accuracy and steady-state amplitude regulation over the shown interval. Additionally, the fundamental component is maintained at 43 Hz with essentially the same magnitude (14.89 A for MPCC and 14.90 A for PI-less MPCC), demonstrating that both approaches preserve the required fundamental current. Importantly, the total harmonic distortion remains unchanged at THD = 20.16 % in both cases, which implies that the dominant distortion mechanisms are not mitigated nor exacerbated by eliminating the PI regulator. Overall, Fig. 7 suggests that the PI-less MPCC preserves the core current tracking behavior of the conventional MPCC under steady-state operation, achieving practically identical fundamental regulation and the current THD performance.

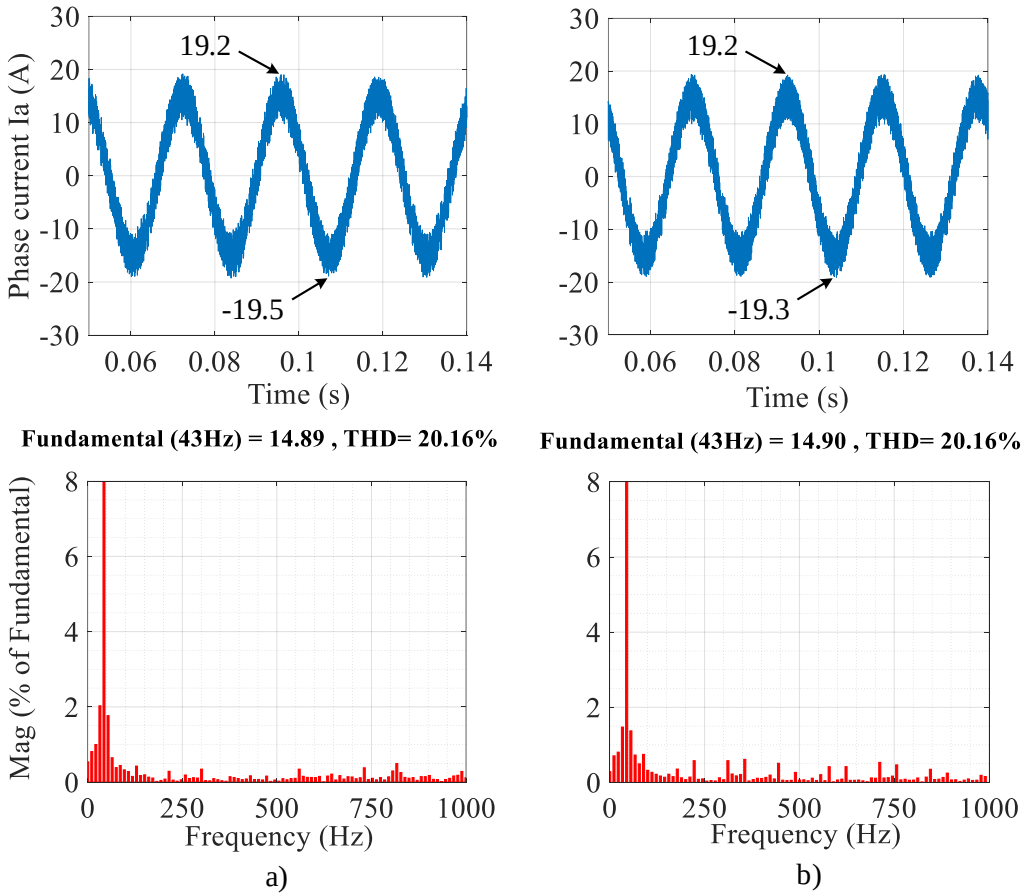


Figure 7: Current THD: a) MPCC and b) the PI-less MPCC

Figure 8 and Table 2 present a quantitative comparison between the conventional MPCC and the proposed PI-less MPCC in terms of electromagnetic torque response and RMS torque ripple over four operating segments. In this study, the RMS torque ripple is adopted to quantify the fluctuation level of the electromagnetic torque. It is defined as the root-mean-square value of the deviation of the instantaneous electromagnetic torque from its average value T_{avg} over the considered time interval. In both cases, the two controllers successfully track the imposed load torque transitions from 10 Nm to 20 Nm and then to 5 Nm, indicating that the elimination of the PI regulator does not degrade the basic torque control function in the steady-state torque quality. As reported in Table 2, the RMS torque ripple is reduced from 1.38 to 1.33 Nm in Segment 1, from 1.45 to 1.36 Nm in Segment 2, from 1.40 to 1.37 Nm in Segment 3, and from 1.44 to 1.41 Nm in Segment 4. These results demonstrate that the proposed strategy achieves ripple reduction in all evaluated operating regions. The largest improvement appears in Segment 2, where the torque ripple decreases by 0.09 Nm, while the other segments also exhibit consistent, though smaller, reductions. Therefore, the PI-less MPCC preserves the fast torque tracking capability of the conventional MPCC while providing improved ripple suppression and smoother electromagnetic torque, which confirms its superior overall control performance under varying load conditions. This tendency indicates that removing the PI loop simplifies the control structure without sacrificing torque regulation accuracy, and it may offer a more attractive solution for applications requiring reduced computational burden together with enhanced steady-state torque characteristics.

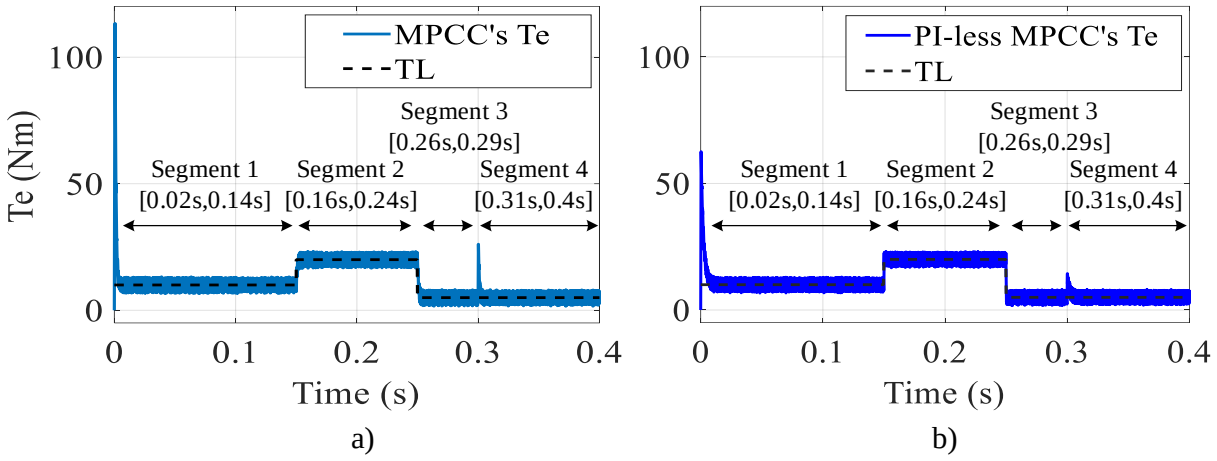


Figure 8: The electromagnetic torque response: a) the MPCC b) the PI-less MPCC

Table 2. RMS Torque ripple

Segment	Load Torque (Nm)	MPCC's *RMS Torque ripple (Nm)*	PI-less MPCC's *RMS Torque ripple (Nm)*
Segment 1	10	1.38	1.33
Segment 2	20	1.45	1.36
Segment 3	5	1.4	1.37
Segment 4	5	1.44	1.41

Overall, the results in Figs. 7 and 8 indicate that removing the PI stage does not degrade the torque regulation and the current THD: the mean torque remains aligned with T_L, and the THD remains comparable to the baseline MPCC. The small reduction in peak excursions observed in the PI-less MPCC suggests a marginal improvement in the electromagnetic torque ripple containment.

4.2. PMSM dynamic performance evaluation

The dynamic performance is evaluated through the speed, electromagnetic torque, and phase current responses during start-up, speed transitions, and load-torque variations. Fig. 9 illustrates the transient behavior of the drive under the MPCC (Fig. 9(a)) and the PI-less MPCC (Fig. 9(b)), showing the speed tracking, the electromagnetic torque versus load torque, and the phase current. In both cases, the controller regulates the motor speed to follow the reference value and maintains torque balance with the applied load steps. In the simulation results, the PI gains were tuned to obtain the best stable transient response under the same operating conditions.

In terms of speed response, PI-less MPCC exhibits lower overshoot and lower peak current under the tested conditions, although the response time is slightly longer. First, the start-up transient of the conventional MPCC in Fig. 9(a) is very fast, reaching the reference in about 0.002 s, but it exhibits a clear overshoot of approximately 83 rad/s. In contrast, the PI-less MPCC in Fig. 9(b) reaches the same reference with a monotonic response and no evident overshoot, although the transient duration is longer at about 0.01 s. Next, when a 10 Nm load is applied at t = 0.15 s, the speed under the conventional MPCC drops to approximately 68 rad/s, whereas the proposed method maintains the speed close to 70 rad/s. Finally, for the subsequent reference speed change step at 0.3 s, both methods tracked the new steady-state speed with similar final accuracy. These results show that the main advantage of the PI-less MPCC lies in its ability to suppress overshoot during start-up and load disturbances. Regarding the electromagnetic torque and the phase current responses during transient, the faster MPCC acceleration is achieved at the cost of substantially higher torque and current peaks. The electromagnetic torque exhibits a start-up peak of approximately 113 Nm for MPCC, whereas the PI-less MPCC limits the peak to about 62 Nm. A similar

trend is observed in the phase current response: the MPCC produces a peak current of about 167 A, whereas the PI-less MPCC limits the peak to about 93 A. After the transient, both controllers settle into a similar operating regime where T_e oscillates around T_L and the phase current returns to its periodic steady-state waveform. The results clearly demonstrate the trade-off between dynamic performance and response time. Although the conventional MPCC provides a faster response, it also produces substantially larger torque and current peaks, whereas the PI-less MPCC yields smoother start-up and load-transition behavior.

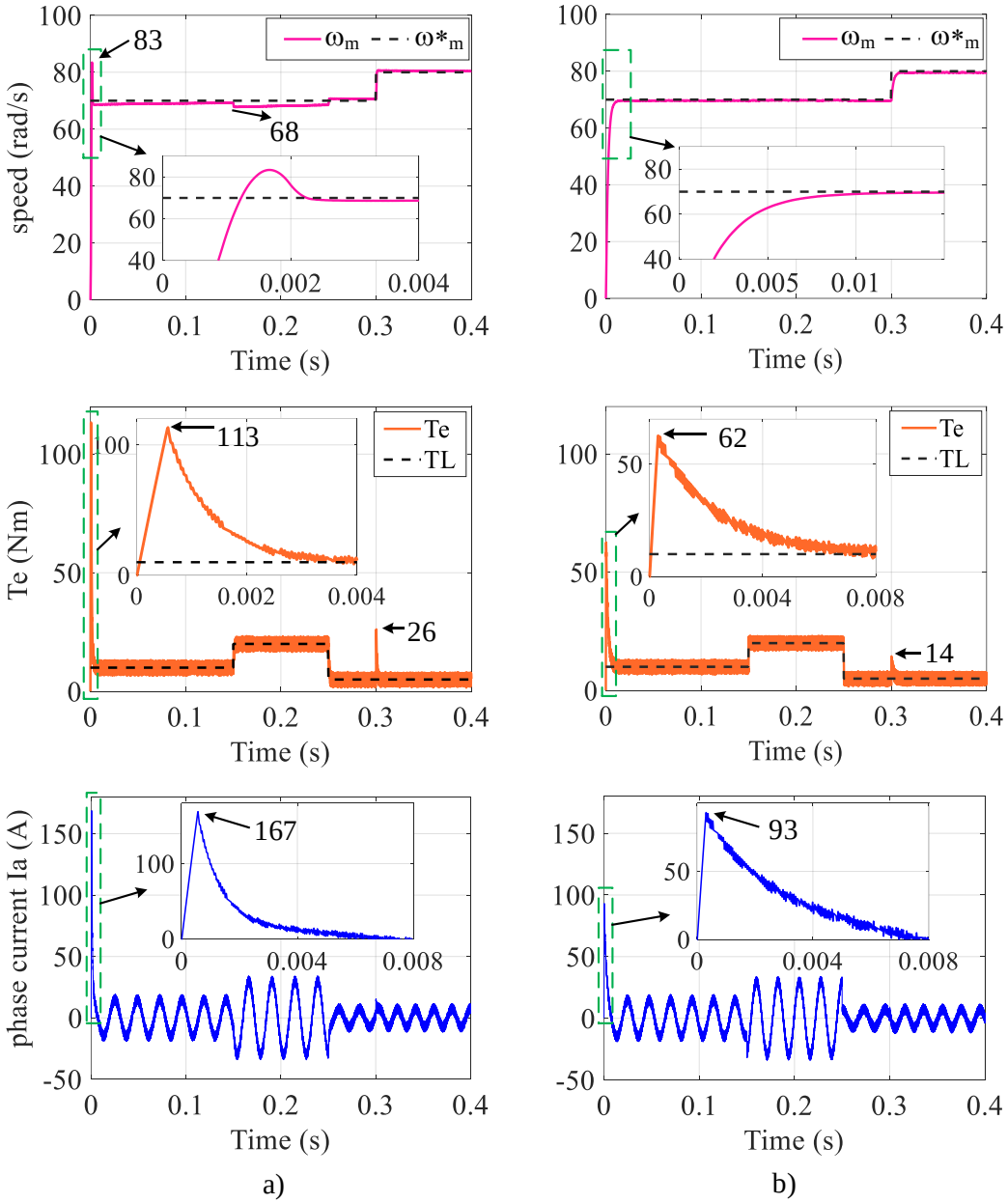


Figure 9: The transient response: a) the MPCC b) the PI-less MPCC

Overall, these results indicate a trade-off between dynamic aggressiveness and actuation stress: the conventional MPCC delivers a faster speed response but induces larger overshoot and significantly higher speed, torque, and current peaks, while the PI-less MPCC provides a more damped and smoother transient

response with reduced speed, torque, and current peaks. The proposed controller can be advantageous for lowering device stress and mitigating mechanical shock during rapid operating point changes.

4.3. Relative computational cost in Simulink

The total computational times of both algorithms, recorded using the MATLAB/Simulink/Debug block, are shown in Fig. 10(a) and Fig. 10(b).

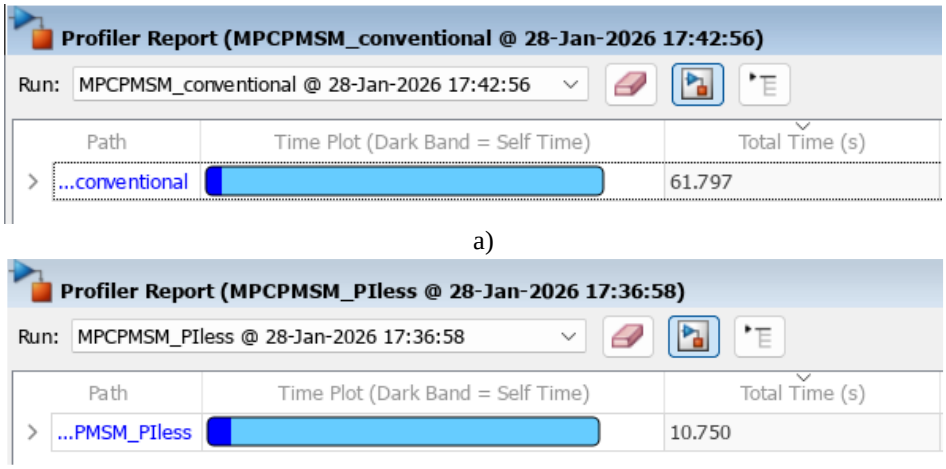


Figure 10: Relative computational cost comparison in MATLAB/Simulink under the same solver and simulation environment: (a) conventional MPCC and (b) PI-less MPCC.

The computational cost shown in Fig. 10 is intended as a relative comparison between the investigated control algorithms under an identical simulation framework. Specifically, both methods were evaluated using the same MATLAB/Simulink environment, the same solver, the same sampling configuration, and the same model settings. Under these identical conditions, the PI-less MPCC demonstrates a lower computational cost than the conventional MPCC, indicating improved computational efficiency in the Simulink-based assessment. The conventional MPCC requires a total execution time of about 62 s (Fig. 10(a)), whereas the PI-less MPCC completes in 11 s (Fig. 10(b)) under the same profiling conditions. This corresponds to an 82% reduction in runtime and a 5.8-fold speedup for the PI-less formulation. The observed improvement shows that the proposed method simplifies the control structure.

5 CONCLUSIONS

Across the steady-state and transient evaluations, the PI-less MPCC preserves the core regulation capability of the conventional MPCC while significantly reducing transient actuation stress. In steady state, both methods deliver nearly identical phase-current amplitude, fundamental component magnitude, and the same THD (20.16%), indicating that removing the PI stage does not change the harmonic quality under the tested operating point. Electromagnetic torque regulation is also comparable, with the PI-less MPCC showing only a marginal reduction in torque ripple. Its main benefit appears in the transient regime, where removing the outer PI loop avoids the additional tuning-dependent dynamics and reduces aggressive current demand during start-up and load changes. As a result, the proposed method achieves lower speed overshoot, lower peak torque, and lower peak current, at the cost of a slightly slower rise time and the need for load-torque information in the speed prediction stage.

Table 3. The key metrics

Parameters	MPCC	PI-less MPCC
Peak speed during start-up (rad/s)	83	0
The starting torque (Nm)	113	62
The starting current (A)	167	93

The torque overshoot at 0.3 s (Nm)	26	14
The total computational time (s)	62	11

During transients, the main difference lies in the dynamic trade-off summarized in Table 3. The MPCC provides a faster and more aggressive response but introduces speed overshoot and much higher torque and current peaks. The PI-less MPCC yields a smoother and better-damped response, and substantially lowers peak electromagnetic torque and phase current, which is beneficial for reducing converter stress and mechanical shock, at the expense of a slightly slower rise.

However, several limitations should be noted. First, the present study only considers operating speeds below 100 rad/s; therefore, the effectiveness of the proposed method at higher speeds remains unverified. Second, the controller assessment was carried out only in the MATLAB/Simulink environment with a sampling frequency of 100 kHz, so the reported computational cost should be understood as a relative simulation-based comparison rather than a hardware execution benchmark. Third, the load torque was assumed to be directly available in Simulink, and practical issues such as estimation error, measurement delay, implementation complexity, and real-time experimental constraints were not considered. Future work will therefore focus on higher-speed analysis and experimental validation.

Overall, the PI-less MPCC offers comparable steady-state current quality, lower transient torque/current peaks, and significantly lower computational cost, making it a promising candidate for PMSM drive applications that require smooth transients and efficient implementation.

ACKNOWLEDGMENT

This article is part of the research project No. 25BCND04, funded by Industrial University of Ho Chi Minh City.

REFERENCES

[1] X. Li, Y. Wang, X. Guo, X. Cui, Sh. Zhang, Y. Li, “An Improved Model-Free Current Predictive Control Method for SPMSM Drives,” IEEE Access vol. 9, pp. 134672 - 134681, 2021.

[2] L. Guo, Y. Wang, H. Wang, Z. Zhang, “Design of high power density double-stator permanent magnet synchronous motor,” *IET Electric Power Applications,* vol. 17, no. 4, pp. 421–431, 2023.

[3] N. D. Quang, V. N. Giap, B. D. Quang, and V. H. Phuong, “Research On Torque Control Of Permanent Magnet Synchronous Motor Application For Electric Vehicle Drive System,” HaUI Journal of Science and Technology, vol. 60, no. 9, pp. 75–79, 2024.

[4] X. Fang, Sh. Lin, X. Wang, Zh. Yang, F. Lin, Zh. Tian, “Model Predictive Current Control of Traction Permanent Magnet Synchronous Motors in Six-Step Operation for Railway Application,” *IEEE Transactions on Industrial Electronics,* vol. 69, no. 9, pp. 8751-8759, 2022.

[5] J. Yang, J. Chen, W. Liu, G. Yang, Ch. Zhang, “Research on Torque Characteristics of the PMSM With the Same Number of Poles and Slots,” *IEEE Transactions on Transportation Electrification,* vol. 11, no. 1, pp. 3028 - 3036, 2025.

[6] D. Mohanraj, J. Gopalakrishnan, B. Chokkalingam, L. M. Popa, “Critical aspects of electric motor drive controllers and mitigation of torque ripple—Review,” *IEEE Access,* vol. 10, pp. 73635-73674, 2022.

[7] S. B. R. Carter, P. Praveen, N. S. V. Varadhan, S. Kowshik, and G. Gopinath, “Field-Oriented Control (FOC) for Permanent Magnet Synchronous Motors (PMSM) In Electric Vehicle ” *2023 IEEE International Conference on Next Generation Electronics (NEleX 2023)*, pp. 1–5, 2023.

[8] M. S. KhajueeZadeh, “Comprehensive Investigation of the Resolver’s Eccentricity Effect on the Field-Oriented Control of PMSM,” *IEEE Sensors Journal* vol. 23, no. 17, pp. 19145 - 19152, 2023.

[9] W. Deng, J. Tang, W. Cheng, "An Enhanced Rotating Vector-Based Direct Torque Control for Matrix Converter-Fed PMSM Drives Using Virtual Pulsating Vectors," *CPSS Transactions On Power Electronics And Applications,* vol. 8, no. 1, pp. 65-73, 2023.

[10] M. H B, P. V, A. Begum, "Direct Torque Control Based Jelly Fish Algorithm For Torque Ripple Reduction in Permanent Magnet Synchronous Motor," *2023 International Conference on Network, Multimedia and Information Technology (NMITCON),* 2023.

[11] K. Li, J. Ding, X. Sun, X. Tian "Overview of Sliding Mode Control Technology for Permanent Magnet Synchronous Motor System," *IEEE Access,* vol. 12, pp. 71685-71704, 2024.

[12] Y. Zuo, Ch. Lai, K. L. V. Iyer, "A Review of Sliding Mode Observer Based Sensorless Control Methods for PMSM Drive," *IEEE Transactions On Power Electronics,* vol. 38, no. 9, pp. 11352-11367, 2023.

[13] M. L. Parvathy, V. K. Thippiripati, "A Simplified Voltage Vector Preselection-Based Multivector Predictive Current Control for Improved Torque Performance of PMSM Drive," *IEEE Transactions On Power Electronics,* vol. 38, no. 7, pp. 8775-8785, 2023.

[14] M. A. Khamis, A. A. Ahmed, A. M. Omara, "Performance Enhancement of SPMSM Under Finite Control Set Model Predictive Current Control," *24th International Middle East Power Systems Conference (MEPCON),* 2023.

[15] X. Wu, M. Yang, T. Wu, K. Lu, Y. Wang, X. Liu, Sh. Huang, H. Cui, "Parameter-Free Predictive Torque and Flux Control for PMSM Based on Incremental Stator Flux Predictive Model," *IEEE Transactions on Industrial Informatics,* vol. 20, no. 2, pp. 2715 - 2726, 2024.

[16] Y. Xu, Y. Zhang, Q. Gao, Zh. Yin, "A Wide-Speed Range Three-Vector-Based Model Predictive Flux Control With Improved Predictive Model for PMSM Drives," *IEEE Transactions on Transportation Electrification* vol. 10, no. 2, pp. 2689-2700, 2024.

[17] M. Zhao, Y. Cao, Ch. Li, Zh. Wang, T. Shi, Ch. Xia, "Expanded Limit Boundary Explicit Model Predictive Direct Speed Control for PMSMs," *IEEE Transactions on Power Electronics,* vol. 39, no. 5, pp. 6089-6101, 2024.

[18] M. Yang, X. Wu, Sh. Huang, W. Liao, T. Wu, Y. Wang, Sh. Huang "Enhanced Model-Free Predictive Speed Control Without Weighting Factors for PMSM Based on Newly Designed Cost Function," *IEEE Transactions On Transportation Electrification,* vol. 10, no. 3, pp. 5703-5714, 2024.

[19] K. Zhang, M. Fan, Y. Yang, Z. Zhu, C. Garcia, J. Rodriguez, "Field Enhancing Model Predictive Direct Torque Control of Permanent Magnet Synchronous Machine," *IEEE Transactions on Energy Conversion* vol. 36, no. 4, pp. 2924-2933, 2021.

[20] I. D. D. Martin, A. Brosch, F. Tinazzi, M. Zigliotto, "Continuous Control Set Model Predictive Torque Control With Minimum Current Magnitude Criterion for Synchronous Motor Drives," *IEEE Transactions on Industrial Electronics,* vol. 71, no. 7, pp. 6787 - 6796, 2024.

[21] L. Xu, Y. Deng, H. Li, C. Zhai, W. Li, and H. Cao, "Model Predictive Current Control of PMSM With Enhanced Robustness Against Parameter Mismatch," *2025 IEEE International Conference on Predictive Control of Electrical Drives and Power Electronics (PRECEDE)* Nanjing, China, pp. 1–6, 2025.

[22] K. Yang, H. Li, and S. Li, "Composite model predictive current control for PMSM servo system," *Transactions of the Institute of Measurement and Control*, vol. 48, no. 6, pp. 1147–1154, 2026.

[23] J. Rodriguez, C. Garcia, A. Mora, F. F. Bahamonde, et al, "Latest Advances of Model Predictive Control in Electrical Drives—Part I: Basic Concepts and Advanced Strategies," *IEEE Transactions on power electronics*, vol. 37, no. 4, pp. 3927-3942, 2022.

[24] Z. Q. Zhu, X. M. Wu, *Sensorless Control of Permanent Magnet Synchronous Machine Drives*, IEEE Press Series on Control Systems Theory and Applications Series, 2023.

[25] X. Wang, H. Cao, H. Sun, P. Wang, "Simplified Algorithm for Multi-Step Model Predictive Control of Permanent Magnet Synchronous Motors for Ship Propulsion," *IEEJ Transactions on Electrical and Electronic Engineering*, vol. 20, no. 8, pp. 1268–1281, Aug. 2025.

TỐI ƯU HÓA HIỆU SUẤT HỆ TRUYỀN ĐỘNG PMSM BẰNG ĐIỀU KHIỂN DÒNG ĐIỆN DỰ ĐOÁN KHÔNG PI

BẠCH THANH QUÝ [1,*], VĂN THỊ KIỀU NHI [1], NGUYỄN ĐẠI VĨ [1]

[1] *Khoa Công nghệ Kỹ thuật Điện, Trường Đại học Công nghiệp Thành Phố Hồ Chí Minh*

* *Tác giả liên hệ: bachthanhquy@iuh.edu.vn*

Tóm tắt. Bài báo này trình bày một chiến lược điều khiển dòng điện dự đoán cho hệ truyền động động cơ đồng bộ nam châm vĩnh cửu (PMSM) nhằm loại bỏ bộ điều chỉnh tỷ lệ-tích phân (PI) để giảm gánh nặng tính toán thường liên quan đến phương pháp điều khiển dòng điện dự đoán truyền thống (MPCC). Bộ điều khiển được xây dựng từ mô hình toán học của PMSM và được rời rạc hoá bằng phương pháp Euler, cho phép chọn điện áp tối ưu cho động cơ mà không dùng bộ điều khiển PI. Bằng cách loại bỏ bộ điều khiển PI này, thuật toán đề xuất giảm thời gian tính toán trong khi vẫn duy trì hiệu suất điều khiển về chất lượng dòng điện và độ mượt mô-men điện từ. Hiệu quả của phương pháp MPCC không PI được đề xuất được đánh giá trên mô hình PMSM 1,5 kW triển khai trong MATLAB/Simulink. Kết quả so sánh với phương pháp MPCC thông thường cho thấy phương pháp đề xuất giảm đáng kể khối lượng tính toán cho bài toán dự đoán dòng điện. Cụ thể, trong cùng điều kiện hoạt động, thời gian tính toán của thuật toán đề xuất là 11 s trong khi thời gian này của phương pháp MPCC thông thường là 62 s. Đồng thời, phương pháp mới này giúp tốc độ bám sát giá trị tham chiếu và giảm đáng kể các độ vọt lố khi tải và tốc độ thay đổi. Nhìn chung, nghiên cứu cho thấy bộ điều khiển MPCC không PI được đề xuất đạt được sự cân bằng tốt giữa hiệu quả tính toán và hiệu suất điều khiển, cho thấy tiềm năng ứng dụng thực tiễn của phương pháp này cho các hệ truyền động PMSM thực tế.

Từ khóa. động cơ đồng bộ nam châm vĩnh cửu, phương pháp điều khiển dòng điện dự đoán, khối lượng tính toán, vectơ điện áp tối ưu.

Received on March 03 – 2026
Revised on April 29 – 2026